Inclusive production of Higgs boson in the two-photon channel at the LHC within k_t-factorization approach and with the Standard Model couplings

Antoni Szczurek,[1,2,*] Marta Łuszczak,[2,†] and Rafał Maciuła[1,‡]

[1] *Institute of Nuclear Physics PAN, PL-31-342 Kraków, Poland*

[2] *University of Rzeszów, PL-35-959 Rzeszów, Poland*

(Dated: July 29, 2014)

arXiv:1407.4243v2 [hep-ph] 28 Jul 2014

Abstract

We calculate differential cross sections for Higgs boson and/or two-photon production from intermediate (virtual) Higgs boson within the formalism of k_t-factorization. The off-shell $g^*g^* \to H$ matrix elements are used. We compare results obtained with infinite top fermion (quark) mass and with finite mass taken into account. The latter effect is rather small. We compare results with different unintegrated gluon distributions from the literature. Two methods are used. In the first method first Higgs boson is produced in the $2 \to 1$ $gg \to H$ k_t-factorization approach and then isotropic decay with the Standard Model branching fraction is performed. In the second method we calculate directly two photons coupled to the virtual Higgs boson. The results of the two methods are compared and differences are discussed. The results for two photons from the Higgs boson are compared with recent ATLAS collaboration data. In contrast to a recent calculation the leading order $gg \to H$ contribution is rather small compared to the ATLAS experimental data ($\gamma\gamma$ transverse momentum and rapidity distributions) for all unintegrated gluon distributions from the literature. We include also higher-order contribution $gg \to H(\to \gamma\gamma)g$, $gg \to gHg$ and the contribution of the W^+W^- and Z^0Z^0. The $gg \to Hg$ mechanism gives similar cross section as the $gg \to H$ mechanism. We argue that there is almost no double counting when adding $gg \to H$ and $gg \to Hg$ contributions due to different topology of Feynman diagrams. The final sum is comparable with the ATLAS two-photon data. We discuss uncertainties related to both the theoretical approach and existing UGDFs.

PACS numbers: 12.38.Bx, 14.80.Bn, 14.70.Bh, 13.85.Qk, 12.38.-t

*Electronic address: antoni.szczurek@ifj.edu.pl

†Electronic address: luszczak@univ.rzeszow.pl

‡Electronic address: rafal.maciula@ifj.edu.pl

I. INTRODUCTION

The Higgs-like boson has been discovered recently at the LHC [1]. It has been observed in a few decay channels. The $\gamma\gamma$ and $Z^0 Z^{0,*}$ are particularly spectacular [2–5]. Before the discovery many of the Higgs properties were strongly dependent on its mass. Now knowing the Higgs boson mass $M_H \approx 126$ GeV we can fix parameters for production and decay of the Higgs boson, at least within the Standard Model. We slowly enter era of more detailed studies. In particular, it is very important to know what is the Higgs boson spin and parity and if it is Standard Model object. Also understanding the rapidity and transverse momentum distributions is particularly interesting. While the total cross section is well under control and was calculated in leading-order (LO), next-to-leading order (NLO) and even next-to-next-to-leading order (NNLO) approximation [6] the distribution in the Higgs boson transverse momentum is more chalanging. This can be addressed e.g. in transverse momentum resummation approach (see e.g. Refs. [7, 8] and references therein).

It was advocated recently that precise differential data for Higgs boson in the two-photon final channel could be very useful to test and explore unintegrated gluon distribution functions (UGDFs) [9]. It was shown very recently [10] that the k_t-factorization formalism with commonly used UGDFs (Kimber-Martin-Ryskin (KMR) [11] and Jung CCFM [12]) gives a reasonable description of recent ATLAS data obtained at $\sqrt{s} = 8$ TeV [13]. We perform similar calculation and, as will be seen in the following, draw rather different conclusions.

In the present study we present several differential distributions for the Higgs boson and photons from the Higgs boson decay at $\sqrt{s} = 8$ TeV for various UGDFs from the literature, also the ones used in the context of low-x physics (Kutak-Staśto [14] and Kutak-Sapeta [15]). We include both leading-order and next-to-leading order contributions. We shall critically discuss uncertainties and open problems in view of the recent ATLAS data.

II. FORMALISM

A. Higgs boson production

In the k_t-factorization approach the cross section for the Higgs boson production can be written somewhat formally as:

$$\sigma_{pp\to H} = \int \frac{dx_1}{x_1}\frac{dx_2}{x_2}\frac{d^2q_{1t}}{\pi}\frac{d^2q_{2t}}{\pi} \quad \delta\left((q_1+q_2)^2 - M_H^2\right)\sigma_{gg\to H}(x_1,x_2,q_1,q_2) \times \mathcal{F}_g(x_1,q_{1t}^2,\mu_F^2)\mathcal{F}_g(x_2,q_{2t}^2,\mu_F^2)\;, \tag{2.1}$$

where $\mathcal{F}_g$ are so-called unintegrated (or transverse-momentum-dependent) gluon distributions and $\sigma_{gg\to H}$ is $gg \to H$ (off-shell) cross section. The situation is illustrated diagramatically in Fig. 1.

It is easy to show in the collinear approximation (see e.g. Ref. [16]) that:

$$\sigma_{gg\to H} = \frac{\pi}{\hat{s}}\delta(\hat{s} - m_H^2)\;. \tag{2.2}$$

After some manipulation the formula (2.1) can be written conveniently as (see Ref. [17])

$$\sigma_{pp\to H} = \int dy d^2p_t d^2q_t \frac{1}{sx_1x_2}\frac{1}{m_{t,H}^2}\overline{|\mathcal{M}_{g^*g^*\to H}|^2}\mathcal{F}_g(x_1,q_{1t}^2,\mu_F^2)\mathcal{F}_g(x_2,q_{2t}^2,\mu_F^2)/4\;, \tag{2.3}$$

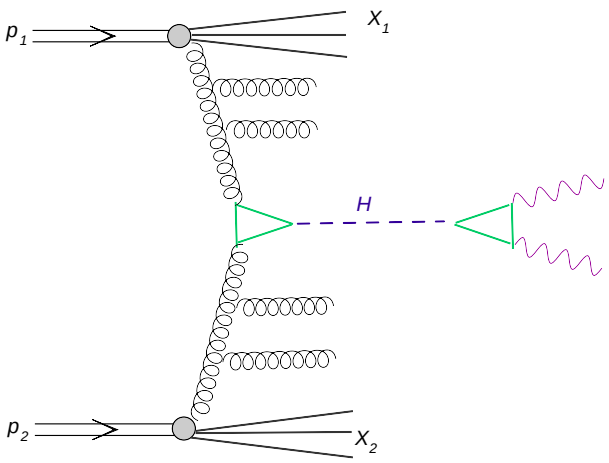

FIG. 1: Dominant leading-order diagram for inclusive Higgs boson production in the two-photon channel.

which can be also used to calculate rapidity and transverse momentum distribution of the Higgs boson.

In the last equation: $\vec{p}_t = \vec{q}_{1t} + \vec{q}_{2t}$ is transverse momentum of the Higgs boson and $\vec{q}_t = \vec{q}_{1t} - \vec{q}_{2t}$ is auxiliary variable which is used in the integration. Furthermore: $m_{t,H}$ is the so-called Higgs transverse mass and $x_1 = \frac{m_{t,H}}{\sqrt{s}} \exp(y)$, $x_2 = \frac{m_{t,H}}{\sqrt{s}} \exp(-y)$. The factor $\frac{1}{4}$ is the jacobian of transformation from $(\vec{q}_{1t}, \vec{q}_{2t})$ to $(\vec{p}_t, \vec{q}_t)$ variables.

Similar formalism was used in the past for production of gauge bosons [19]. There gluon distributions have to be replaced by unintegrated quark and antiquark distributions.

Let us concentrate for a while on the matrix element for the $g^*g^* \to H$. In Ref. [17] the on-shell matrix element was used. In Ref. [20] the off-shell matrix element was used instead, however in the approximation of infinitly heavy top in the triangle-coupling of gluons to the Higgs boson (see also[18] where the off-shell matrix element was discussed). Then the effective $g^*g^* \to H$ coupling is relatively simple. The matrix element under discussion (for on-shell Higgs boson) takes the simple form:

$$\mathcal{M}^{ab}_{g^*g^* \to H} = -i\delta^{ab} \frac{\alpha_s}{4\pi} \frac{1}{v} \left(m_H^2 + p_t^2\right) cos(\phi) \frac{2}{3} \,, \tag{2.4}$$

where $v^2 = \left(G_F \sqrt{2}\right)^{-1}$. The effect of finite-mass corrections was studied in Ref. [21] in the context of k_t-factorization and in [22] in the context of higher-order collinear approximation corrections. Then the corresponding matrix element is more complicated and can be written with the help of two form factors:

$$\mathcal{M}^{ab}_{g^*g^* \to H} = -i\delta^{ab} \frac{\alpha_s}{4\pi} \frac{1}{v} \left[\left(m_H^2 + p_t^2\right) cos(\phi) G_1(q_1, q_2, q) - \frac{2(m_H^2 + p_t^2)^2 |q_{1t}||q_{2t}|}{(m_H^2 + q_{1t}^2 + q_{2t}^2)} G_2(q_1, q_2, q) \right] . \tag{2.5}$$

The form factors G_1 and G_2 have an integral representation. However, at not too big virtualities of gluons and Higgs boson the following approximate formula for the G_1 and G_2

form factors can be used [21]:

$$G_1 \;=\; \frac{2}{3}\left(1+\frac{7}{30}\chi+\frac{2}{21}\chi^2+\frac{11}{30}(\xi_1+\xi_2)+...\right)\;, \tag{2.6}$$

$$G_2 \;=\; -\frac{1}{45}(\chi-\xi_1-\xi_2)-\frac{4}{315}\chi^2+....\;, \tag{2.7}$$

where the expansion variables χ, ξ_1, ξ_2 above are defined as:

$$\chi \;=\; \frac{q^2}{4m_f^2}\;, \tag{2.8}$$

$$\xi_1 \;=\; \frac{q_1^2}{4m_f^2}<0\;, \tag{2.9}$$

$$\xi_2 \;=\; \frac{q_2^2}{4m_f^2}<0\;. \tag{2.10}$$

B. $H\to\gamma\gamma$

The matrix element for the Higgs boson decay into photons with helicity λ_1 and λ_2 can be written as

$$\mathcal{M}_{H\to\gamma\gamma}(\lambda_1,\lambda_2)=T^{\mu\nu}_{H\to\gamma\gamma}\epsilon^*_\mu(\lambda_1)\epsilon^*_\nu(\lambda_2)\;. \tag{2.11}$$

The leading-order (LO) vertex function can be decomposed as the sum

$$T^{\mu\nu}_{H\to\gamma\gamma}=T^{\mu\nu,W}_{H\to\gamma\gamma}+T^{\mu\nu,t}_{H\to\gamma\gamma}+...\;, \tag{2.12}$$

where the first term includes loops with intermediate $W^\pm$ and the second term triangle(s) with top quarks. The dots represent contribution of triangles with bottom and charm quarks and with τ leptons, etc. The vertex function can be written as:

$$T^{\mu\nu}_{H\to\gamma\gamma}(p_1,p_2)=i\frac{\alpha_{em}}{2\pi}\mathcal{A}\left(G_F\sqrt{2}\right)^{1/2}(p_2^\mu p_1^\nu-(p_1\cdot p_2)g^{\mu\nu})\;. \tag{2.13}$$

In the Standard Model the $\mathcal{A}$ constant is:

$$\mathcal{A}=\mathcal{A}_W(\tau_W)+N_c e_f^2\mathcal{A}_t(\tau_t)+... \tag{2.14}$$

where the arguments are:

$$\tau_W=\frac{m_H^2}{4m_W^2}\quad,\quad \tau_t=\frac{m_H^2}{4m_t^2}\;. \tag{2.15}$$

The functions $\mathcal{A}_W$ and $\mathcal{A}_t$ have the simple form:

$$\mathcal{A}_W(\tau) \;=\; -\left(2\tau^2+3\tau+3(2\tau-1)f(\tau)\right)/\tau^2\;, \tag{2.16}$$

$$\mathcal{A}_t(\tau) \;=\; 2\left(\tau+(\tau-1)f(\tau)\right)/\tau^2\;, \tag{2.17}$$

where the function $f(\tau)$ reads:

$$f(\tau)=arcsin^2(\sqrt{t})\;. \tag{2.18}$$

For light fermions the function $f(\tau)$ is slightly different [23].

The two-photon decay width can be calculated as:

$$\Gamma_{H\to\gamma\gamma} = \frac{1}{32\pi^2}\Sigma_{\lambda_1\lambda_2}|\mathcal{M}_{H\to\gamma\gamma}(\lambda_1,\lambda_2)|^2\frac{p}{m_H^2}\frac{1}{2} \; . \tag{2.19}$$

The factor $\frac{1}{2}$ is due to identity of the final state photons. Using Eq.(2.19) with matrix element given by Eq.(2.11) we get $\Gamma_{H\to\gamma\gamma} = 0.91 \times 10^{-5}$ which, when combined with the total decay width $\Gamma_H \approx 4$ MeV [25], gives branching fraction $\mathrm{BF}_{H\to\gamma\gamma} = 2.27 \times 10^{-3}$, consistent with what is known from the literature (see e.g. Ref. [26]). Using the decay matrix element from Ref. [10] would give much bigger $\mathrm{BF}_{H\to\gamma\gamma} \sim 0.01$ (incorrect) branching fraction. Two-loop corrections are rather very small [28].

C. $g^*g^* \to H^* \to \gamma\gamma$

Let us combine now all elements defined above and write matrix element for the $g^*g^* \to H^* \to \gamma\gamma$ process.

$$\mathcal{M}_{g^*g^*\to H^*\to\gamma\gamma}(\lambda_1,\lambda_2) = \mathcal{M}_{g^*g^*\to H^*}(\vec{q}_{1t},\vec{q}_{2t};\hat{s})\frac{1}{\hat{s}-M_H^2+i\Gamma_H M_H}\mathcal{M}_{H^*\to\gamma\gamma}(\lambda_1,\lambda_2) \; . \tag{2.20}$$

In the infinitly heavy quark approximation the matrix element squared averaged over colors can be written in the quite compact way (see Ref. [10]):

$$\overline{|\mathcal{M}|^2} = \frac{1}{1152\pi^4}\alpha_{em}^2\alpha_s^2 G_F^2|\mathcal{A}|^2\frac{\hat{s}^2(\hat{s}+p_t^2)^2}{(\hat{s}-m_H^2)^2+m_H^2\Gamma_H^2}\cos^2(\phi) \; . \tag{2.21}$$

The differential (in photon rapidities y_1, y_2 and transverse momenta p_{1t}, p_{2t}) cross section for the production of a pair of photons from the $g^*g^* \to H^* \to \gamma\gamma$ subprocess with intermediate virtual Higgs boson can be written as:

$$\begin{aligned}\frac{d\sigma(pp\to HX\to\gamma\gamma X)}{dy_1dy_2d^2p_{1t}d^2p_{2t}} &= \frac{1}{16\pi^2\hat{s}^2}\cdot\frac{1}{2}\cdot\int\frac{d^2k_{1t}}{\pi}\frac{d^2k_{2t}}{\pi}\overline{|\mathcal{M}^{off}_{g^*g^*\to H^*\to\gamma\gamma}|^2} \\ &\times\ \delta^2\left(\vec{k}_{1t}+\vec{k}_{2t}-\vec{p}_{1t}-\vec{p}_{2t}\right)\mathcal{F}_g(x_1,k_{1t}^2,\mu^2)\mathcal{F}_g(x_2,k_{2t}^2,\mu^2) \; . \end{aligned} \tag{2.22}$$

Please note that in this case the $m_H^2+p_t^2$ term in Eq.(2.4) for on shell Higgs boson is replaced by $\hat{s}+p_t^2$ for virtual Higgs boson. This has consequences some distance from the resonance position where the cross section is however small. In principle, also M_H^2 in definition of the $\mathcal{A}$ functions should be replaced by $\hat{s}$ here.

Since we integrate over full phase space in y_1, y_2, p_{1t} and p_{2t} we have to include in addition identity factor $\frac{1}{2}$, in full analogy to the calculation of the decay width into two photons.

How to remove the δ function in Eq.(2.22) in a convenient for calculation way is described in Ref. [29]. The calculation of the cross section according to formula (2.22) with matrix element (2.21) is not easy as the light Higgs boson discovered recently is a very narrow resonance. This calculation is performed within a Monte Carlo method using a well know package VEGAS [30]. We have carefully tested both numerics and convergence.

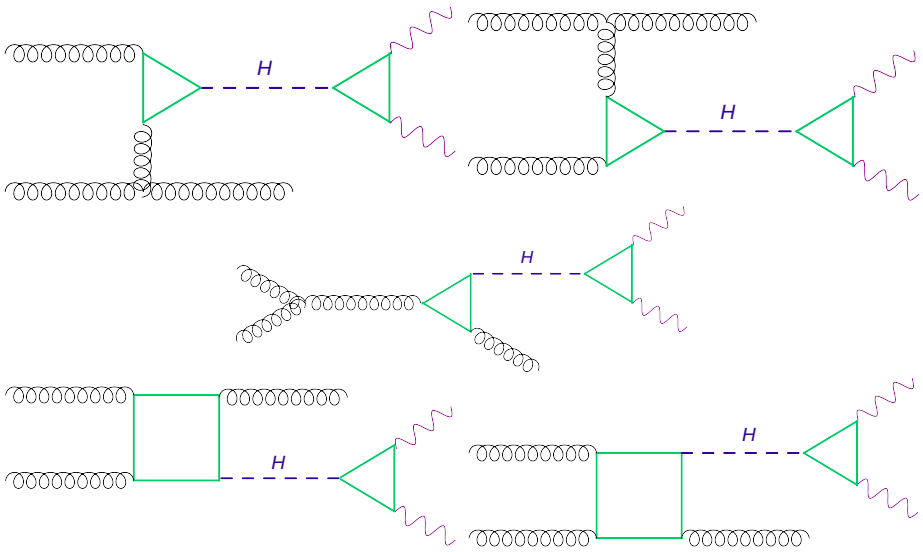

FIG. 2: Typical diagrams for QCD NLO contributions to the Higgs boson production.

D. $gg \to Hg$

In the collinear-approximation the cross section for fixed-order processes of the type $p_1 p_2 \to H p_3$ (parton1+parton2 $\to$ Higgs+parton3) (see Fig. 2) of the order of α_s is well known since long time [31].

The corresponding cross section differential in Higgs boson rapidity (y_H), associated parton rapidity (y_p) and transverse momentum of each of them can be written as:

$$\begin{aligned}\frac{d\sigma}{dy_H dy_p d^2p_t}(y_H, y_p, p_t) &= \frac{1}{16\pi^2 \hat{s}^2} \times \Big\{ x_1 g_1(x_1,\mu^2) x_2 g_2(x_2,\mu^2) \overline{|\mathcal{M}_{gg\to Hg}|^2} \\ &+ \left[\sum_{f_1=-3,3} x_1 q_{1,f_1}(x_1,\mu^2) \right] x_2 g_2(x_2,\mu^2)\ \overline{|\mathcal{M}_{qg\to Hq}|^2} \\ &+ x_1 g_1(x_1,\mu^2) \left[\sum_{f_2=-3,3} x_2 q_{2,f_2}(x_2,\mu^2) \right] \overline{|\mathcal{M}_{gq\to Hq}|^2} \\ &+ \sum_{f=-3,3} x_1 q_{1,f}(x_1,\mu^2) x_2 q_{2,-f}(x_2,\mu^2) \overline{|\mathcal{M}_{qq\to Hg}|^2} \Big\}. \end{aligned} \quad (2.23)$$

The indices f in the formula above number both quarks ($f > 0$) and antiquarks ($f < 0$). Only three light flavours are included in actual calculations here. The explicit formulae for $\overline{|\mathcal{M}|^2}$ can be found in Ref. [31]. We have checked that the $gg \to Hg$ contribution dominates over the two other types of contributions. This can be understood as due to the presence of the box contributions for $gg \to Hg$ but absent in the other cases.

In the following we shall calculate the dominant $gg \to Hg$ contribution also taking into account transverse momenta of initial gluons. In the k_t-factorization the NLO differential

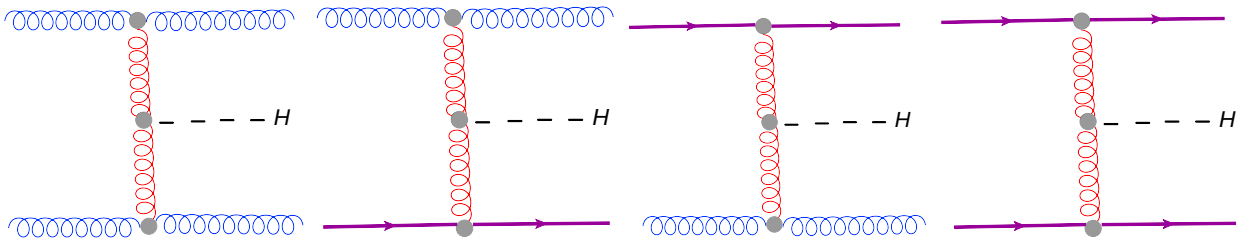

FIG. 3: The $2 \to 3$ diagrams which are used in order to make reference to the $2 \to 1$ k_t-factorization calculation.

cross section can be written as:

$$\frac{d\sigma(pp \to HgX)}{dy_H dy_g d^2p_{H,t} d^2p_{g,t}} = \frac{1}{16\pi^2 \hat{s}^2} \int \frac{d^2q_{1t}}{\pi} \frac{d^2q_{2t}}{\pi} \overline{|\mathcal{M}^{off-shell}_{g^*g^* \to Hg}|^2} \times \delta^2\left(\vec{q}_{1t} + \vec{q}_{2t} - \vec{p}_{H,t} - \vec{p}_{g,t}\right) \mathcal{F}(x_1, q_{1t}^2, \mu^2) \mathcal{F}(x_2, q_{2t}^2, \mu^2) \; . \quad (2.24)$$

This can be further simplified as discussed e.g. in Ref. [29].

Calculation of the off-shell matrix element for the process under consideration is rather complicated in the most general case as it involves loops (triangles and boxes). Since the box diagrams with very heavy top quarks/antiquarks dominate at high energies we expect that the off-shell effects should be relatively small. In the present approach we make the following replacement to simplify the calculation:

$$\overline{|\mathcal{M}^{off-shell}_{g^*g^* \to Hg}|^2} \to \overline{|\mathcal{M}^{on-shell}_{gg \to Hg}(s,t,u)|^2} \; , \quad (2.25)$$

where the latter is analytical continuation of the on-shell matrix element off mass shell. The larger q_{1t} or q_{2t} the worse the approximation could be. This cannot be quantified, however, before exact off-shell matrix element is calculated. This goes beyond the scope of the present study.

E. Higgs boson and dijets in the context of k_t-factorization approach

It is well known that in contrast to gauge boson ($W^\pm$ and Z^0) production for calculating inclusive cross section for the Higgs boson production not only LO but also NLO and even NNLO corrections are pretty large. Collinear NNLO contributions to the Higgs boson production associated with dijet production was discussed e.g. in Ref. [37]. A somewhat simplified but pedagogical high-energy approach was discussed in Ref. [38].

In the present analysis we wish to make a reference to the $gg \to H$ k_t-factorization calculations so a simplified approach may be useful. In the following we shall evaluate cross section and differential distributions in the collinear approximation for the subprocesses shown in Fig. 3. At large q_{1t} and q_{2t} (transverse momenta of the exchanged (red online) gluons) the contribution of the first subprocess ($gg \to gHg$) can be directly compared to the k_t-factorization result with the KMR UGDF. This may be useful in order to understand higher-order contributions contained in the k_t-factorization approach.

The matrix element for the $gg \to gHg$ which can (should) be used to compare the collinear factorization result with the k_t-factorization approach result reads:

$$\begin{aligned}\mathcal{M}^{gg\to gHg}_{\lambda_1\lambda_2\to\lambda_3\lambda_4}(ace, bde') = \quad & g_s(\mu^2_{r,1}) f_{ace}\epsilon_{\mu_1}(\lambda_1) C^{\mu_1\nu_1\tau_1}(-p_1, p_3, q_1)\epsilon^*_{\nu_1}(\lambda_3) \\ & \frac{(-ig_{\tau_1\tau_1'})}{t_1} T^{\tau_1'\tau_2'}_{gg\to H}(q_1, q_2, p_H) \frac{(-ig_{\tau_2\tau_2'})}{t_2} \\ & g_s(\mu^2_{r,2}) f_{bde'}\epsilon_{\mu_2}(\lambda_2) C^{\mu_2\nu_2\tau_2}(-p_2, p_4, q_2)\epsilon^*_{\nu_2}(\lambda_4) \ , \end{aligned} \tag{2.26}$$

where dependence on renormalization scale was made explicit.

Here the matrix element is evaluated as in Ref. [38] using high-energy approximations. It can be written somewhat schematically as:

$$\overline{|\mathcal{M}_{gg\to gHg}|^2} = 4\frac{C_A^2}{N_c^2-1} g_s^2(\mu^2_{r,1}) g_s^2(\mu^2_{r,2}) \frac{\hat{s}}{t_1^2 t_2^2} |C_{gg\to H}(q_1, p_H, q_2)|^2 \ . \tag{2.27}$$

The matrix element is particularly simple in the limit:

$$s_{ij} \gg s_{iH}, s_{jH} \gg m_H^2 \ . \tag{2.28}$$

We have made explicit running of strong coupling constant in (2.27). In practical calculation it is reasonable to take $\mu^2_{r,1} = p^2_{3t}$ and $\mu^2_{r,2} = p^2_{4t}$. At high energies $t_1 \approx -q^2_{1t} = -p^2_{3t}$ and $t_2 \approx -q^2_{2t} = -p^2_{4t}$.

The phase space integration is performed then with the $gg \to gHg$ matrix element squared and collinear gluon distribution functions (GDFs), see for example next subsection. Both integrated and differential cross sections can be then compared with those obtained within the k_t-factorization approach. Especially inspiring is to understand the interrelation between the two approaches for larger jet/Higgs transverse momenta p_{3t}, p_{4t}, p_{tH}.

In the high-energy approach quark and antiquarks contributions can be easily included by replacing gluon distributions $g(x_1, \mu^2_{f,1})$ and $g(x_2, \mu^2_{f,2})$ by so-called effective parton distributions (see e.g. Ref. [40]):

$$\begin{aligned} f_{eff}(x_k, \mu_k^2) \ &= \ g(x_k, \mu^2) \\ &+ \ \frac{C_F}{C_A}\left(u(x_k, \mu_k^2) + d(x_k, \mu_k^2) + s(x_k, \mu_k^2) + \bar{u}(x_k, \mu_k^2) + \bar{d}(x_k, \mu_k^2) + \bar{s}(x_k, \mu_k^2)\right) \ . \end{aligned} \tag{2.29}$$

Similar procedure is often done in the context of Mueller-Navelet jets. We shall evaluate and show the quark/antiquark components separately as they are not taken into account explicitly in the k_t-factorization approach.

F. *WW* fusion

Now we wish to consider purely electroweak corrections that are known to give sizeable contribution to the Higgs boson production.

The second most important mechanism for the Higgs boson production is the fusion of off-shell gauge bosons: WW or ZZ. It is known that at the LHC energy the WW fusion constitutes about $10-15\%$ of the integrated inclusive cross section. If the weak boson fusion

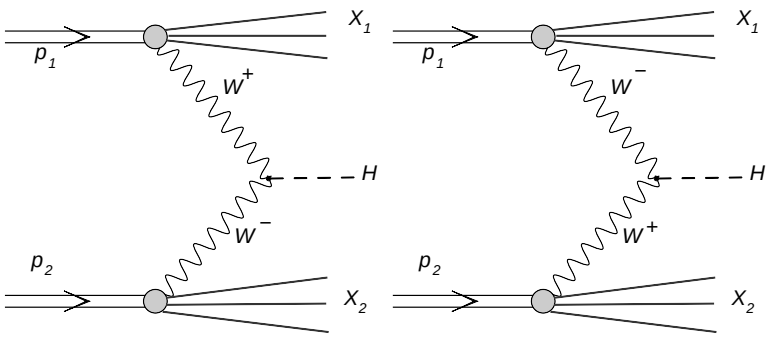

FIG. 4: Diagrams for the WW fusion.

contribution was separated, the measurement of the WWH (or ZZH) coupling would be very interesting test of the Standard Model.

In the present paper we are interested in differential distributions of Higgs boson rather than in the integrated cross section.

For the gauge boson fusion the partonic subprocess is of the $2 \to 3$ type: $q(p_1) + q(p_2) \to q(p_3) + q(p_4) + H(p_H)$ (see Fig. 4).

The corresponding proton-proton cross section can be written as

$$d\sigma = \mathcal{F}_{12}^{VV}(x_1, x_2)\, \frac{1}{2\hat{s}}\, \overline{|\mathcal{M}_{qq\to qqH}|^2}\, \frac{d^3p_3}{(2\pi)^3 2E_3} \frac{d^3p_4}{(2\pi)^3 2E_4} \frac{d^3p_H}{(2\pi)^3 2E_H} \times (2\pi)^4 \delta^4(p_1 + p_2 - p_3 - p_4 - p_H)\, dx_1 dx_2\ . \tag{2.30}$$

The next-to-leading order corrections to the matrix element of the WW fusion are rather small [32]. The leading-order subprocess matrix element was calculated first in Ref. [33]. The spin averaged matrix element squared reads

$$\overline{|\mathcal{M}|^2} = 128\sqrt{2} G_F^3 \frac{M_W^8 (p_1 \cdot p_2)(p_3 \cdot p_4)}{(2p_3 \cdot p_1 + M_W^2)^2 (2p_4 \cdot p_2 + M_W^2)^2}\ . \tag{2.31}$$

For the WW fusion, limiting to light flavours, the partonic function is

$$\begin{aligned} &\mathcal{F}_{12}^{WW}(x_1, x_2) = \\ &\left(u_1(x_1,\mu_1^2) + \bar{d}_1(x_1,\mu_1^2) + \bar{s}_1(x_1,\mu_1^2)\right)\left(\bar{u}_2(x_2,\mu_2^2) + d_2(x_2,\mu_2^2) + s_2(x_2,\mu_2^2)\right) + \\ &\left(\bar{u}_1(x_1,\mu_1^2) + d_1(x_1,\mu_1^2) + s_1(x_1,\mu_1^2)\right)\left(u_2(x_2,\mu_2^2) + \bar{d}_2(x_2,\mu_2^2) + \bar{s}_2(x_2,\mu_2^2)\right)\ . \end{aligned} \tag{2.32}$$

In the following we take $\mu_1^2 = \mu_2^2 = M_H^2$. It is convenient to introduce the following new variables:

$$\begin{aligned} \vec{p}_+ &= \vec{p}_3 + \vec{p}_4\ , \\ \vec{p}_- &= \vec{p}_3 - \vec{p}_4\ , \end{aligned} \tag{2.33}$$

which allow to eliminate the momentum-dependent $\delta^3(...)$ in Eq.(2.30). Instead of integrating over x_1 and x_2 we shall integrate over $y_1 \equiv \ln(1/x_1)$ and $y_2 \equiv \ln(1/x_2)$. Then using Eq.(2.30) we can write the inclusive spectrum of Higgs boson as

$$\begin{aligned} \frac{d\sigma}{dy d^2p_t} = \int dy_1 dy_2\ x_1 x_2 \mathcal{F}(x_1, x_2, \mu_1^2, \mu_2^2)\, \frac{1}{2\hat{s}} \frac{d^3p_-}{16}\, \overline{|\mathcal{M}_{qq\to qqH}|^2}\, \frac{1}{2E_3}\, \frac{1}{2E_4} \\ \times\ \frac{1}{(2\pi)^5}\, \delta(E_1 + E_2 - E_3 - E_4 - E_H)\ . \end{aligned} \tag{2.34}$$

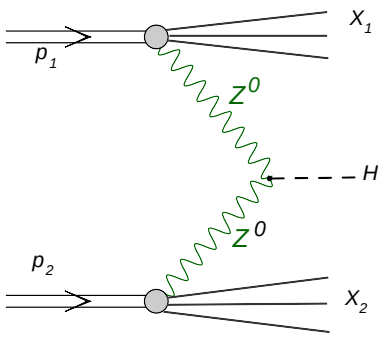

FIG. 5: Typical diagram for the ZZ fusion.

This is effectively a four-dimensional integral which can be calculated numerically.

Strong and electroweak corrections to the Higgs boson production via vector-boson fusion at the LHC were calculated e.g. in Ref. [34] and in Ref. [35]. The corrections are relatively small and in the following analysis we shall show only leading-order results as a reference to the k_t-factorization result.

G. ZZ fusion

The ZZ fusion (see Fig. 5) can be calculated in an analogous way.

The corresponding matrix element depends on the subprocess type (set of quark, anti-quark flavours). It can be written as [33]:

$$\overline{|\mathcal{M}|^2_{f_1 f_2}} = 128\sqrt{2} G_F^3 M_Z^8 \frac{C_1^Z(f_1 f_2)(p_1 \cdot p_2)(p_3 \cdot p_4) + C_2^Z(f_1 f_2)(p_1 \cdot p_4)(p_2 \cdot p_3)}{(2p_3 \cdot p_1 + M_Z^2)^2 (2p_4 \cdot p_2 + M_Z^2)^2} \,. \tag{2.35}$$

The flavour dependent coefficients read:

$$\begin{aligned} C_1^Z(f_1 f_2) &= \frac{1}{4}\left((V_{f_1} - A_{f_1})^2 (V_{f_2} - A_{f_2})^2 + (V_{f_1} + A_{f_1})^2 (V_{f_2} + A_{f_2})^2\right) \,, \\ C_2^Z(f_1 f_2) &= \frac{1}{4}\left((V_{f_1} - A_{f_1})^2 (V_{f_2} + A_{f_2})^2 + (V_{f_1} + A_{f_2})^2 (V_{f_2} - A_{f_2})^2\right) \,. \end{aligned} \tag{2.36}$$

The V_f and A_f are well known vector and axial-vector couplings of the Z^0 boson to quarks/antiquarks. They can be expressed in terms of third component of the weak isospin, charge of quark/antiquark and sinus of the Weinberg angle.

The differential cross section is calculated in exactly the same way as for the WW fusion.

H. Associated production with W and Z bosons

For completeness one could include also production of the Higgs boson associated with gauge bosons W^+, W^- and Z^0. These are formally lower-order ($2 \to 2$) processes than the WW and ZZ fusion ($2 \to 3$) processes considered above. They were first considered in Ref. [36].

The matrix elements are very simple:

$$|\mathcal{M}_{f_1 f_2 \to WH}|^2 = \frac{(G_F M_W^2)^2}{72\pi^2} |V_{f_1 f_2}|^2 \frac{3M_W^2 + p_W^2}{(\hat{s} - M_W^2)^2} ,$$
$$|\mathcal{M}_{ff \to ZH}|^2 = \frac{(G_F M_Z^2)^2}{72\pi^2} (V_f^2 + A_f^2) \frac{3M_Z^2 + p_Z^2}{(\hat{s} - M_Z^2)^2} . \quad (2.37)$$

In the equation above p_V is momentum of the gauge boson in the HV center of mass frame:

$$p_W^2 = \frac{1}{4\hat{s}} \left(\hat{s}^2 + M_V^4 + M_H^4 - 2\hat{s}M_V^2 - 2\hat{s}M_H^2 - 2M_V^2 M_H^2 \right) ; \quad (2.38)$$

where $V = W, Z$.

The fully differential cross section can be written as:

$$\frac{d\sigma}{dy_H dy_W d^2p_t} = \frac{1}{16\pi\hat{s}^2} |\mathcal{M}_{f_1 f_2 \to WH}|^2 \times \sum\nolimits_{f_1 f_2} \left(x_1 q_{f_1}(x_1, \mu^2) x_2 \bar{q}_{f_2}(x_2, \mu^2) + x_1 \bar{q}_{f_1}(x_1, \mu^2) x_2 q_{f_2}(x_2, \mu^2) \right) ,$$
$$\frac{d\sigma}{dy_H dy_Z d^2p_t} = \frac{1}{16\pi\hat{s}^2} |\mathcal{M}_{ff \to ZH}|^2 \times \sum\nolimits_{f} \left(x_1 q_f(x_1, \mu^2) x_2 \bar{q}_f(x_2, \mu^2) + x_1 \bar{q}_f(x_1, \mu^2) x_2 q_f(x_2, \mu^2) \right) . \quad (2.39)$$

The Higgs boson distributions can be obtained from those above by integrating over y_W and y_Z, respectively.

III. RESULTS

A. $gg \to H$ and subsequent $H \to \gamma\gamma$ decay

In Table I we present total (integrated over full phase space) cross section for the $2 \to 1$ gluon-gluon fusion mechanism for several UGDFs from the literature at $\sqrt{s} = 8$ TeV. For reference the leading-order collinear approximation result is typically 5-7 pb depending somewhat on parton distribution functions used in the calculation. The k_t-factorization results (for several UGDFs used here) are somewhat smaller. There are two reasons for this. First, when calculating gluon longitudinal momentum fractions transverse momentum of the Higgs boson is included which increases x_1 and x_2 and therefore lowers the cross section. Secondly, many low-x UGDF do not apply and/or are too small in the region of $x_1, x_2 > 0.01$. Quite different cross sections are obtained for different UGDFs. This shows that the UGDFs (often fitted only to HERA data) are much more uncertain than the collinear gluon distribution functions (GDF) fitted to many sets of high-energy data. However, UGDFs have advantage that they can be used for correct (exclusive) kinematics including transverse momenta of initial gluons, which cannot be addressed properly in collinear calculations.

For comparison in the middle block we show contribution of $ij \to iHj$ processes calculated in the collinear-factorization approach for the jet transverse momenta bigger than 10 GeV. The $gg \to gHg$ contribution is of similar size as that for the leading order $gg \to H$ k_t-factorization approach. We think that the latter contribution is to large extent contained in the calculation with the KMR UGDF. However, the quark and antiquark initiated contributions which are also fairly large (~ 0.6 pb) must be included in addition explicitly.

TABLE I: The cross section for Higgs production $p_t < 400$ GeV in pb for $\sqrt{s} = 8$ TeV and for different UGDFs from the literature. For comparison we show also contribution of the $gg \to gHg$ and $ij \to iHj$ processes ($p_{1t}, p_{2t} > 10$ GeV), and WW and ZZ fusion.

contribution	$\mu_r^2 = \mu_f^2 = m_H^2$
KMR	5.2349
Jung CCFM (set$A0$)	8.2705
Jung CCFM (set$A+$)	12.3791
Jung CCFM (set$A-$)	5.7335
Kutak-Staśto	2.6074
Kutak-Sapeta	1.5465
KMR, q_{1t}, $q_{2t} > 10$ GeV	2.4585
$gg \to gHg$, $q_{1t}, q_{2t} > 10$ GeV	0.24
$ij \to iHj$, $q_{1t}, q_{2t} > 10$ GeV	0.57
WW fusion	0.9332
ZZ fusion	0.02641

At the very bottom we show contributions of the WW and ZZ fusions. The electroweak contribution is quite sizeable. As will be shown below they play important role at large Higgs boson transverse momenta.

The so different cross sections obtained with different UGDFs may be partially understood by looking at distribution in x_1 or x_2 (see Fig. 6). The KMR UGDF gives much larger contribution in the region of $x_1, x_2 > 0.01$ than the typically small-x UGDFs. The other UGDFs are in this range of x's not very realistic.

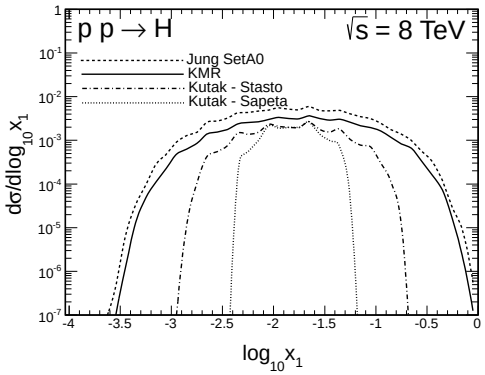

FIG. 6: Distribution in $\log_{10}(x_1)$ or $\log_{10}(x_2)$ for $gg \to H$ and for different UGDFs used in the present analysis.

In addition, the different UGDFs in the literature has quite different dependence on gluon transverse momenta. This is well demonstrated in Fig. 7 where we show two-dimensional maps in $q_{1t} \times q_{2t}$ for different UGDFs. The Kutak-Sapeta UGDF gives a sharp peak at large q_{1t} and q_{2t}. This means that using such an UGDF one cannot obtain large Higgs boson transverse momenta. Quite large gluon transverse momenta ($q_{1t}, q_{2t} \sim m_H$) enter the production of the Higgs boson for the KMR and Jung CCFM (set$A0$) UGDFs. For the

KMR UGDF a clear enhancement at small q_{1t} or q_{2t} can be observed. This is rather a region of nonperturbative nature, where the KMR UGDF is rather extrapolated than calculated. However, we have checked that the contribution of the region when $q_{1t} < 2$ GeV or $q_{2t} < 2$ GeV constitutes only less than 5% of the integrated cross section. This is then a simple estimate of uncertainty of the whole approach.

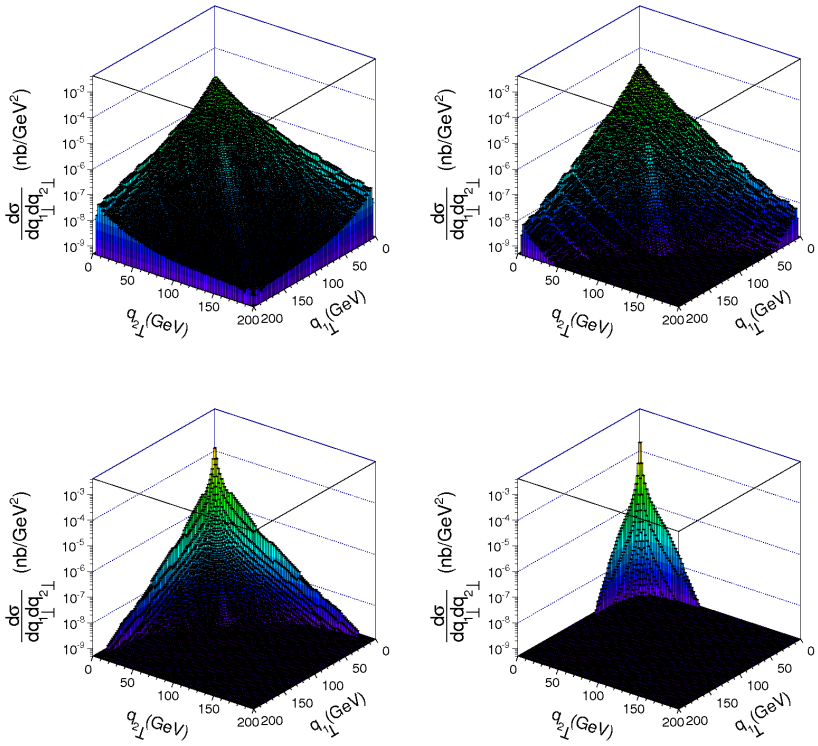

FIG. 7: Distribution in q_{1t} and q_{2t} for $gg \to H$ and for different UGDFs: KMR, Jung CCFM (set$A0$), Kutak-Staśto and Kutak-Sapeta.

Now we can proceed to the production of photons. We start from two-dimensional distributions in $\frac{d\sigma}{dydp_t}$ in rapidity and transverse momentum of the Higgs boson calculated according to Eq.(2.3) and perform its decay isotropically in the Higgs boson rest frame (assuming spin zero of the Higgs boson). Next relativistic boosts are performed to get distributions of photons in the proton-proton center of mass system. As an example in Fig. 8 we show two-dimensional distributions in photon transverse momenta. Also here the distributions for different UGDFs differ significantly. In Fig. 9 we show in addition two examples but in the contour form which shows some details better than the lego plot.

In order to confront our calculations with the preliminary ATLAS data [13] extra cuts on photon rapidities and transverse momenta must be imposed in addition. We require:

$$-2.37 < \eta_{\gamma,1}, \eta_{\gamma,2} < 2.37,$$

$$\max(p_{1t}, p_{2t}) > 0.35 \times M_{\gamma\gamma}, \quad \min(p_{1t}, p_{2t}) > 0.25 \times M_{\gamma\gamma},$$
$$105 \text{ GeV} < M_{\gamma\gamma} < 160 \text{ GeV} \tag{3.1}$$

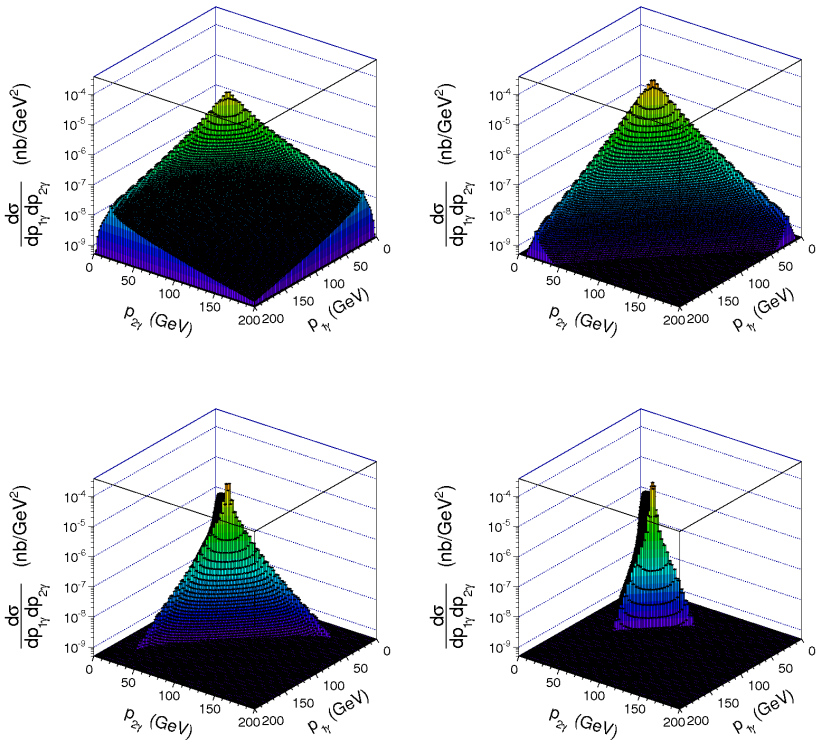

FIG. 8: Distributions in photon transverse momenta p_{1t} and p_{2t} for the $gg \to H$ and for the KMR, Jung CCFM (set$A0$), Kutak-Staśto and Kutak-Sapeta UGDFs.

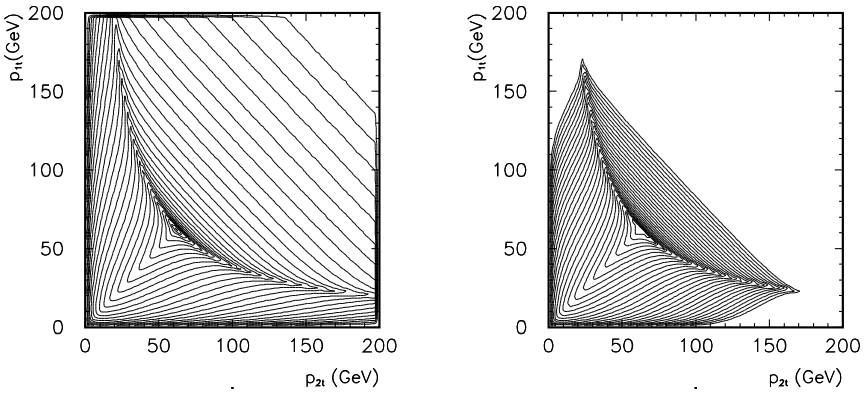

FIG. 9: Distributions in photon transverse momenta p_{1t} and p_{2t} for $gg \to H$ and for the KMR and Jung CCFM (set$A0$) UGDFs for the contour representation.

as relevant for the ATLAS analysis [13]. The distribution in transverse momentum of the photon pair (almost transverse momentum of the Higgs boson) is shown in Fig. 10 for different UGDFs from the literature together with the ATLAS data [13]. The calculated distributions lay much below the ATLAS data in clear disagreement with the recent calculation in Ref. [10]. We shall return to the discussion of the disagreement and its potential

explanation in the rest part of the paper.

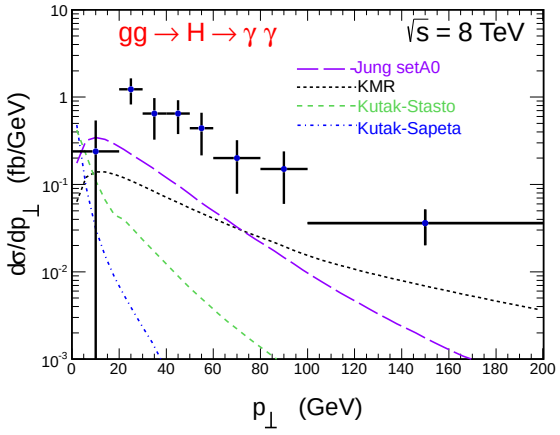

FIG. 10: Transverse momentum distribution of the Higgs boson produced in the $gg \to H$ subprocess in the $\gamma\gamma$ channels for different UGDFs from the literature.

B. $gg \to H^* \to \gamma\gamma$

In this section we shall present results of calculations performed within the k_t-factorization in the second method. The photon distributions from virtual Higgs decay are calculated including correctly kinematics of the $2 \to 2$ subprocess $gg \to H^* \to \gamma\gamma$. Now we wish to compare differential cross sections obtained in this way with those obtained within the first method. Clearly the second method leads to sizeably larger cross sections. This may be helpful in the context of the deficit discussed in the previous section, but certainly not sufficient.

In Fig. 11, as an example, we show somewhat theoretical distribution in $\log_{10}(x_i)$, $i = 1, 2$ for the KMR UGDF with $\mu^2 = m_H^2$. Both low-x ($x < 10^{-2}$) and high-x ($x > 10^{-2}$) regions give similar contributions to the cross section.

In Fig. 12 we show distribution in p_{1t} or p_{2t} (identical) for the two methods. The two distributions are rather similar as far as the shape is considered.

The distribution in $p_{t,sum}$ ($\vec{p}_{t,sum} = \vec{p}_{1t} + \vec{p}_{2t}$) is particularly interesting as it reflects distribution of the Higgs boson and can be measured experimentally. In Fig. 13 we again compare results obtained in the two methods. The shapes obtained with the two methods are practically identical but there is a small difference in the normalization.

Now we wish to show several results for the second approach only. Let us start from single photon transverse momentum distribution. In Fig. 14 we show such distributions for two selected UGDFs. The peak at $p_t \sim m_H/2$ is of kinematical nature. The KMR UGDF leads to larger photon transverse momenta.

Particularly interesting is distribution in two-photon invariant mass. The huge peak at $M_{\gamma\gamma} = M_H$ corresponds to on-shell Higgs boson. We observe (see Fig. 15) small contributions from off-shell Higgs boson configurations with invariant masses both smaller or larger than the on shell (peak) value. The sharp peak shows that the integration of the cross section is not easy. We have, however, carefully checked the convergence.

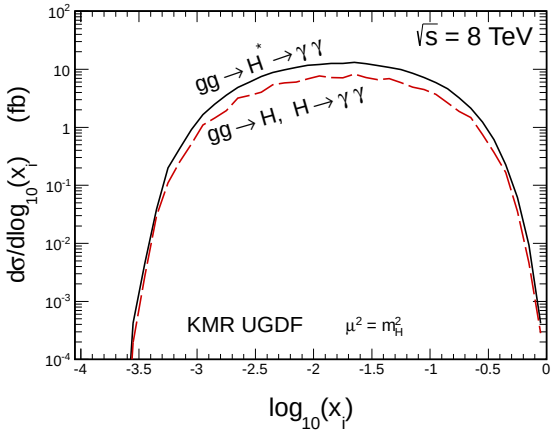

FIG. 11: Distribution in $\log_{10} x_i$ for the KMR UGDF and $\mu^2 = m_H^2$ for first (on-shell Higgs boson, long-dashed line) and second (off-shell Higgs boson, solid line) method.

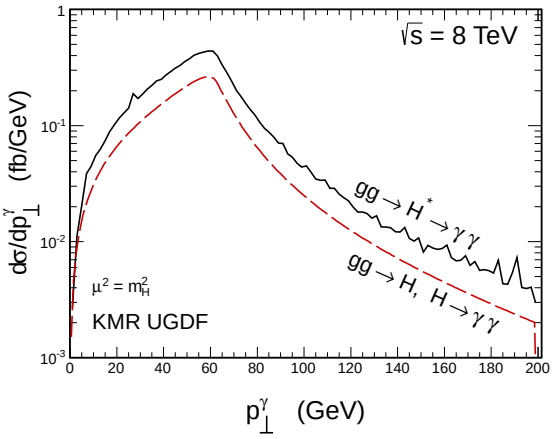

FIG. 12: Distribution in p_{it} (i=1,2) for the KMR UGDF and $\mu^2 = m_H^2$ for the first (long-dashed line) and second (solid line) method.

As was already mentioned, the distribution for $p_{t,sum}$ reflects the Higgs boson transverse momenta. Interesting question is how the distribution is sensitive to the choice of the UGDF model. Figure 16 shows that the KMR UGDF generates much bigger Higgs boson transverse momenta than the Jung CCFM (set$A0$).

Another interesting observable is correlation in azimuthal angle between the outgoing photons (see Fig. 17). A bigger back-to-back correlation is observed for the Jung CCFM (set$A0$) than for the KMR UGDF. This is similar as already observed for azimuthal correlations between $c\bar{c}$ (see e.g. Ref. [45]). The decorrelation for the KMR UGDF is even larger (compare only shapes) than in the soft-gluon transverse momentum resummation [8]. Small $\phi_{\gamma\gamma}$ are strongly correlated with large gluon transverse momenta q_{1t} or q_{2t}. As discussed above this may be overestimated in the k_t-factorization approach with the KMR UGDF.

In Fig. 18 we show rather theoretical distributions in "initial" gluon transverse momenta. Those distributions are almost identical to those discussed already for on-shell Higgs boson production (see Fig. 7). The distribution for the KMR UGDF is broader than that for the

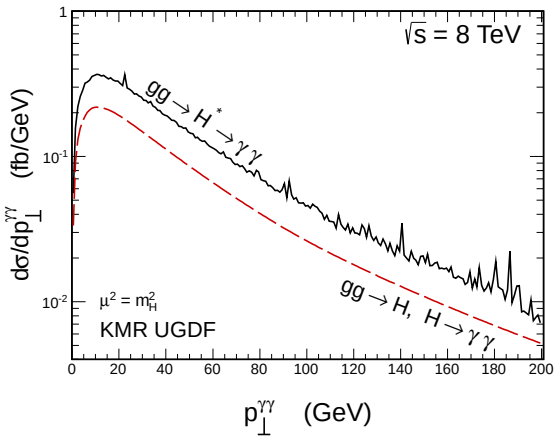

FIG. 13: Distribution in $p_{t,sum}$ for the KMR UGDF and $\mu^2 = m_H^2$ for the first (long-dashed line) and second (solid line) method.

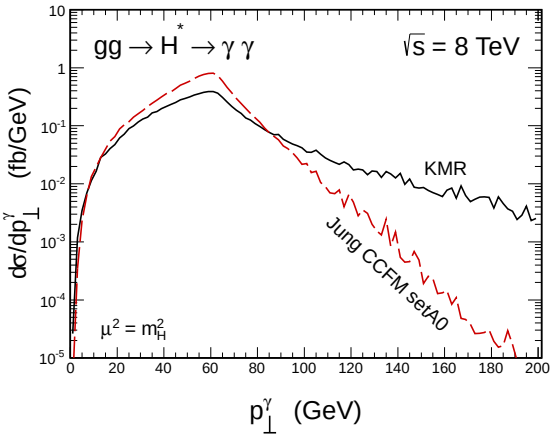

FIG. 14: Distribution of photon transverse momentum for the KMR (solid line) and the Jung CCFM (set$A0$) (long-dashed line) UGDF, for $\mu^2 = m_H^2$.

Jung CCFM (set$A0$) UGDF.

Finally we wish to present two-dimensional correlations in photon transverse momenta (see Fig. 19). Again this distribution is similar to its counterpart obtained within first method (compare Fig. 8).

C. Higgs in association with one jet (gluon)

Now we wish to show some results of calculation for Higgs + gluon production within k_t-factorization approach.

We start from a pedagogical two-dimensional distributions (similar distribution was discussed in the context of the $gg \to H$ mechanism) in initial gluon transverse momenta (q_{1t}, q_{2t}). In Fig. 20 we show distribution for the four different UGDFs used also for the $gg \to H$ calculation.

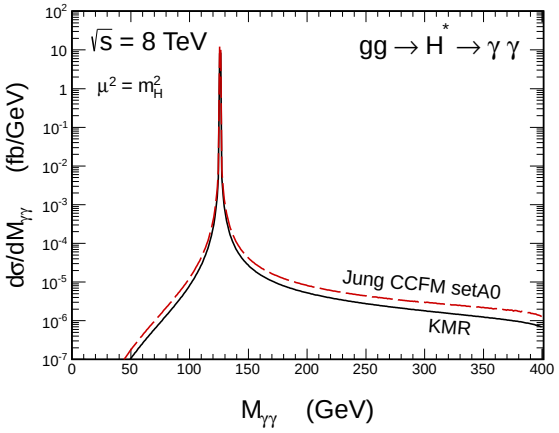

FIG. 15: Distribution of diphoton invariant mass for the KMR (solid line) and the Jung CCFM (set$A0$) (long-dashed line) UGDF, for $\mu^2 = m_H^2$.

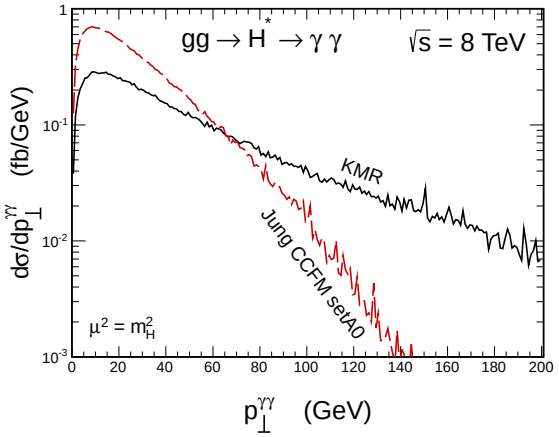

FIG. 16: Distribution of diphoton transverse momentum for the KMR (solid line) and the Jung CCFM (set$A0$) (long-dashed line) UGDF, for $\mu^2 = m_H^2$.

The Higgs transverse momentum distribution is particularly interesting in the context of the preliminary ATLAS data. In Fig. 21 we show corresponding distributions for the four UGDFs used in the present study. It is worth to notice that the inclusion of gluon transverse momenta automatically removes singular behaviour of the cross section at $p_t \to 0$. We observe that the cross section for $gg \to Hg$ is of the same order of magnitude as that calculated before for $gg \to H$. We wish to notice here that in contrast to other gluon initiated processes the dominant piece of the $gg \to Hg$ is not included in the calculation of $gg \to H$. This can be easily understood by inspecting diagrams in Fig. 1 and Fig. 2. While for the $gg \to H$ fusion the triangle with top quarks is the dominant mechanism, in the case of the $gg \to Hg$ process these are the diagrams with top-quark boxes that dominate. Due to their completely different topology the diagrams with boxes are certainly not contained in our previous calculations for the $gg \to H$ fusion. The same is true for all previous calculations of the Higgs boson production in the k_t-factorization [10, 17, 20, 21].

In Fig. 22 we show sum of the leading ($gg \to H$) and the next-to-leading ($gg \to Hg$)

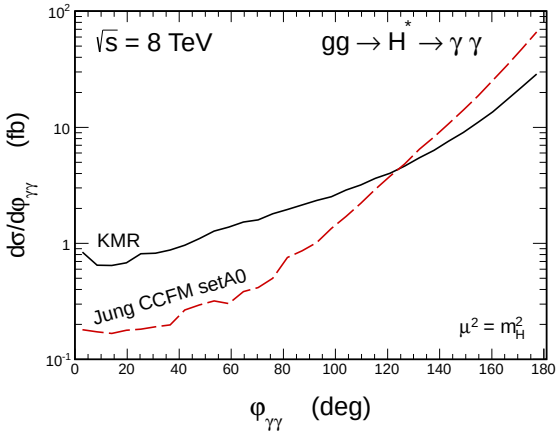

FIG. 17: Distribution of azimuthal angle between photons for the KMR (solid line) and the Jung CCFM (set$A0$) (long-dashed line) UGDF, for $\mu^2 = m_H^2$.

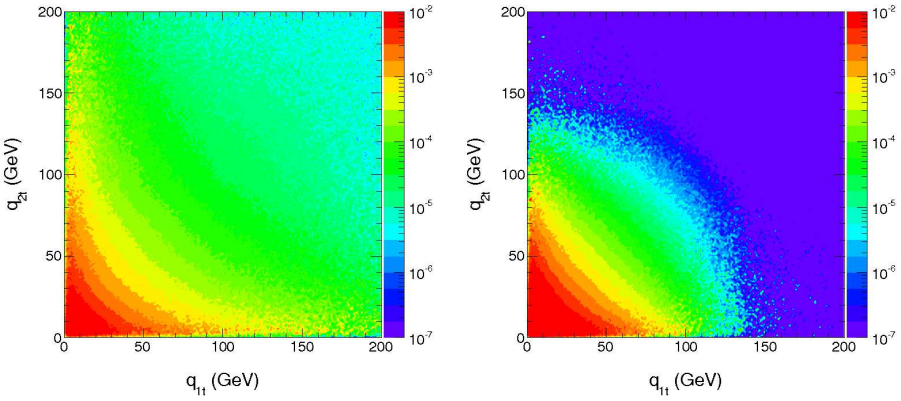

FIG. 18: Two-dimensional distribution in (q_{1t}, q_{2t}) for the KMR (left panel) and for the Jung CCFM (set$A0$) (right panel) UGDF and for $\mu^2 = m_H^2$.

contributions again for the different UGDFs used so far. The result for the KMR and Jung CCFM set$A0$ UGDFs is already almost consistent with the new ATLAS data. The electroweak contribution will be discussed below.

D. Higgs in association of two jets

It is interesting to compare the k_t-factorization calculation at large q_{1t} and q_{2t} (transverse momenta of the fusing gluons) with standard (collinear) calculation of the Higgs boson production associated with two jets. In Fig. 23 we show two dimensional distribution in the space of the transverse momenta of the associated jets (p_{3t}, p_{4t}) for the $gg \to gHg$ process only. Since initial gluons are collinear this is also exactly distribution in (q_{1t}, q_{2t}) (transverse momenta of the t-channel gluons) and can be directly compared with similar distributions obtained previously in the k_t-factorization $gg \to H$ calculation. In this calculation high-energy limit and rapidity ordering (see Ref. [38]) was assumed. The shape here is similar

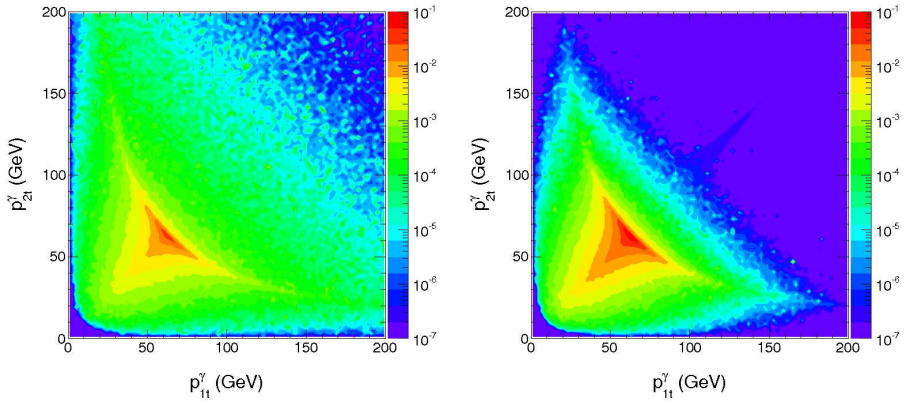

FIG. 19: Two-dimensional distribution in photon transverse momenta (p_{1t}, p_{2t}) for the KMR (left panel) and for the Jung CCFM (set$A0$) (right panel) UGDF and for $\mu^2 = m_H^2$.

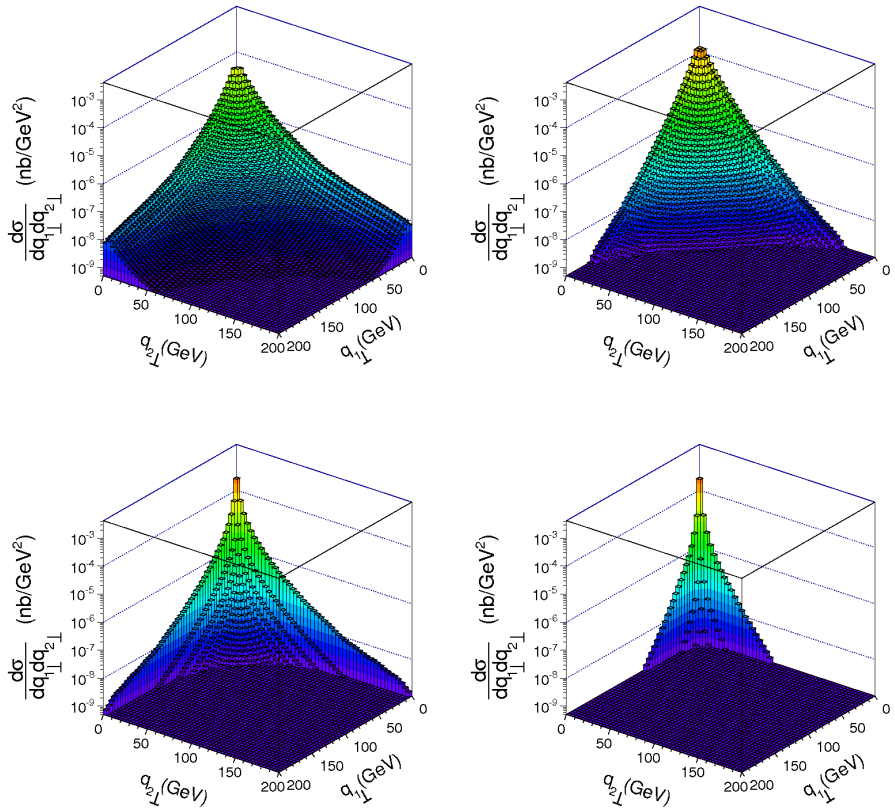

FIG. 20: Two-dimensional distribution in (q_{1t}, q_{2t}) for the $gg \to Hg$ process for the four different UGDFs used previously also for the $gg \to H$ calculation: KMR UGDF and $\mu_F^2 = m_H^2$ (left top panel) and Jung CCFM set$A0$ (right top panel), Kutak-Staństo (left bottom panel) and Kutak-Sapeta (right bottom panel).

to that for the KMR UGDF. However, the absolute normalization is sizeably smaller. We

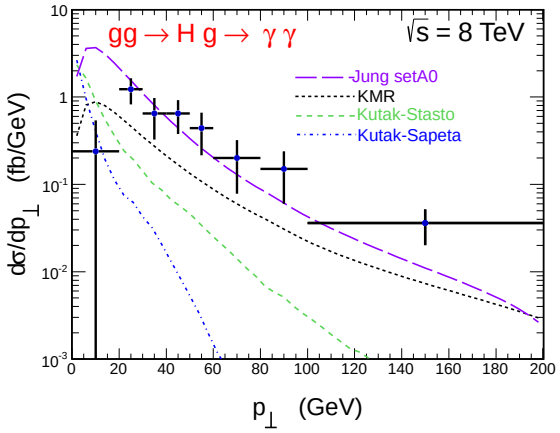

FIG. 21: Transverse momentum distribution of the Higgs boson in the $\gamma\gamma$-channel produced in the $gg \to Hg$ subprocess for the different UGDFs from the literature.

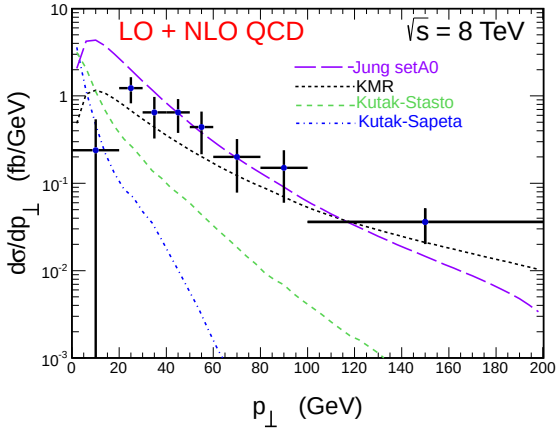

FIG. 22: Transverse momentum distribution of the Higgs boson in the $\gamma\gamma$-channel produced in the $gg \to H$ and in the $gg \to Hg$ subprocesses for the different UGDFs from the literature.

think that such contributions are therefore effectively included in the calculation with the KMR UGDF. But this is certainly not true for saturation-inspired UGDFs.

The contributions of the $gq(\bar{q})$, $q(\bar{q})$ and $(q(\bar{q}), q(\bar{q})$ discussed previously in the formalism section are usually not included explicitly in the k_t-factorization approach with most of UGDFs (except of the KMR UGDF) and has to be taken into account when comparing theoretical results to experimental data.

Let us make further comparison of results for $gg \to gHg$ with $p_{3t}, p_{4t} < 10$ GeV (which automatically means $q_{1t}, q_{2t} < 10$ GeV) with similar result obtained within the k_t-factorization approach for $gg \to H$ with the KMR UGDF. From Table I we see that the result for the KMR UGDF is much bigger than that for the $gg \to gHg$ collinear-factorization approach. This is difficult to understand as in the KMR model the whole transverse momentum is generated in the last step of the ladder. In Fig. 24 we show distributions in $\log_{10}(x_1)$ or $\log_{10}(x_2)$ for both cases. One clearly sees that x's for the k_t-factorization approach (maximum at $\log_{10}(x_i) \approx$ -1) are smaller than their counterparts for the $gg \to gHg$ (maximum

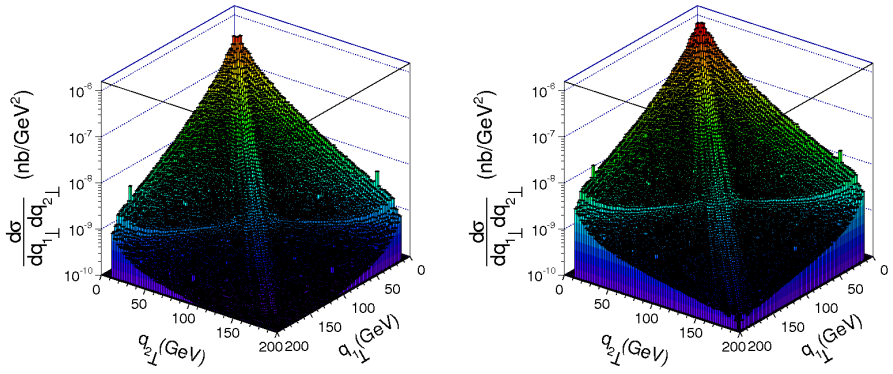

FIG. 23: Two-dimensional distribution in jet transverse momenta (p_{3t}, p_{4t}) for the $2 \to 3$ process $gg \to gHg$ (left) and $ij \to iHj$ (right). In this calculation $\mu_F^2 = m_H^2$ and $\mu_{r,1}^2 = p_{3t}^2$, $\mu_{r,2}^2 = p_{4t}^2$. A cut on $p_{3t}, p_{4t} > 10$ GeV has been assumed in addition.

at $\log_{10}(x_i) \approx$ -2). This explains huge cross section at large q_{1t} and/or large q_{2t} within the k_t-factorization approach for $gg \to H$ which does not include fully correctly the kinematics of the actual process (missing jets are not included in calculating x_1 and x_2). It is not clear to us how to consistently correct the calculation for the kinematical effect.

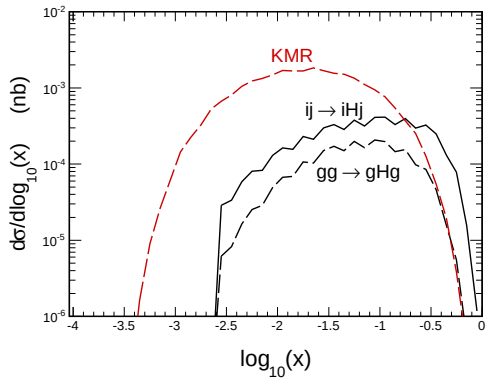

FIG. 24: $\log_{10}(x_i)$ distribution for the k_t-factorization approach for $gg \to H$ (upper dashed line, red online) and for $gg \to gHg$ (lower dashed line) and $ij \to iHj$ (solid line) for $q_{1t}, q_{2t} > 10$ GeV.

E. Other contributions

In Fig. 25 we compare contributions of different mechanisms. The QCD contributions shown in this subsection were calculated with the KMR UGDF. Surprisingly the contribution of the next-to-leading order mechanism $gg \to Hg$ is even slightly bigger than that for the $gg \to H$ fusion, especially for intermediate Higgs boson transverse momenta. As already discussed there is almost no double counting when adding the corresponding cross sections due to quite different Feynman diagram topology. As shown in the present analysis the $gg \to H$ mechanism is not sufficient within the k_t-factorization approach. The $2 \to 3$

contribution of the $gg \to gHg$ subprocess is probably also quite large but here one can expect that a big part is already contained in the $gg \to H$ calculation especially with the KMR UGDF. Therefore we do not add this contribution explicitly when calculating $d\sigma/dp_{t,sum}$. The contribution of the WW, ZZ fusion is also fairly sizeable. In principle, the Higgs bosons (or photons from the Higgs boson) could be to some extend isolated by requiring rapidity gap i.e. production of Higgs boson isolated off other hadronic activity.

If we added the contribution together we would almost describe the ATLAS data.

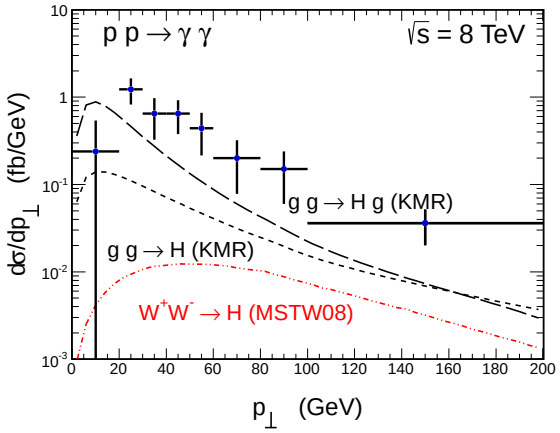

FIG. 25: Transverse momentum distribution of the Higgs boson in the $\gamma\gamma$ channels for different mechanisms: $gg \to H$ (solid line), $gg \to Hg$ (dashed line) and $WW \to H$ (dash-dotted line).

In the future one could include into such an analysis even higher order $gg \to gHg$ contribution as well as associated production $gg \to tH\bar{t}$, $q\bar{q} \to WH$ and $q\bar{q} \to ZH$. Their contributions are known to be only slightly smaller than the contribution of the WW and ZZ fusion.

IV. CONCLUSIONS

In the light of new ATLAS data we have carefully analysed Higgs boson production in the $\gamma\gamma$ channel. We have concentrated rather on QCD contributions. The $gg \to H$ mechanism has been considered within k_t-factorization approach. Different unintegrated gluon distributions from the literature have been used. In general, the cross section for the leading-order Higgs production within k_t-factorization approach is somewhat smaller than its counterpart for the leading-order collinear approximation.

We have calculated the cross section for $gg \to H \to \gamma\gamma$ within two methods. In the first method we have performed decay of the on-shell Higgs boson within a Monte Carlo method using the $H \to \gamma\gamma$ branching fraction known from the literature. In the second method we have performed direct calculation with explicit $2 \to 2$ $gg \to H^* \to \gamma\gamma$ subprocess. In the second method the intermediate Higgs boson is off-mass-shell. The two methods give slightly different results. We have carefully discussed corresponding differences. The second, more proper method leads to a small enhancement of the cross section with respect to the first method. If this is the explanation of the enhancement of the $\gamma\gamma$ channel as observed by the ATLAS and CMS collaborations requires further studies.

In contrast to recent claims in the literature, the leading-order $gg \to H$ calculation does not describe the preliminary ATLAS data when correct Standard Model couplings are taken into account. Higher-order corrections within k_t-factorization such as $gg \to Hg$ have been discussed in addition. Their contribution turned out to be of similar order as that for $gg \to H$. We have argued that there is almost no double counting when adding the leading-order $gg \to H$ and next-to-leading order $gg \to Hg$ contributions in the k_t-factorization approach. The reason is that the box diagrams dominate for the $gg \to Hg$ subprocess and they are not present in the leading-order $gg \to H$ subprocess. Also $ij \to iHj$ $(i, j = q, \bar{q}g)$ collinear NNLO contributions have been shown to be rather sizeable, also those with quarks and/or antiquarks that are certainly not included in the leading-order k_t-factorization approach.

In addition, we have calculated purely electroweak contributions of the WW and ZZ fusion and associated production $qq' \to WH$ and $qq \to ZH$. In general, the electroweak contributions are also not negligible.

The sum of all (QCD and electroweak) contributions gives a result which is almost consistent with the ATLAS preliminary data. This requires, however, a further analysis as some double-counting between the leading ($gg \to H$), next-to-leading ($gg \to Hg$) and NNLO ($gg \to gHg$) order contributions have to be carefully studied in this approach.

In summary, the production of the Higgs boson in the $\gamma\gamma$ channel can be used to test unintegrated gluon distributions provided all contributions to the cross section are carefully taken into account.

Acknowledgments We are indebted to Simone Marzani for information about some references related to our work and Nikolai Zotov for pointing out a misprint in our first manuscript on arXiv. This work was partially supported by the Polish NCN grants: DEC-2011/01/B/ST2/04535 and DEC-2013/09/D/ST2/03724 .

---

[1] G. Aad *et al.* (the ATLAS Collaboration), Phys. Lett. **B716**, 1 (2012);
S. Chatrchyan *et al.* (the CMS Collaboration), Phys. Lett. **B716**, 30 (2012).

[2] G. Aad *et al.* (the ATLAS Collaboration), Phys. Lett. **B726**, 88 (2013); corrigendum: Phys. Lett. **B734**, 406 (2014).

[3] S. Chatrchyan *et al.* (the CMS Collaboration), Phys. Rev. **D89**, 092007 (2014).

[4] V. Khachatryan *et al.* (the CMS Collaboration), arXiv:1405.3455 [hep-ex].

[5] G. Aad *et al.* (the ATLAS Collaboration), arXiv:1406.3827 [hep-ex].

[6] R.V. Harlander and W.B. Kilgore, Phys. Rev. Lett. **88** (2002) 201801;
C. Anastasiou and K. Melnikov, Nucl. Phys. **B646** (2002) 220;
V. Ravindran, J. Smith and W.L. van Neerven, Nucl. Phys. **B665** (2003) 325.

[7] D. de Florian, G. Ferrera, M. Grazzini and D. Tommasini, JHEP **1111** (2011) 064, arXiv:1109.2109 [hep-ph].

[8] D. de Florian, G. Ferrera, M. Grazzini and D. Tommasini, JHEP **1206** (2012) 132, arXiv:1203.6321 [hep-ph].

[9] P. Cipriano, S. Dooling, A. Grebenyuk, P. Gunnellini, F. Hautmann, H. Jung and P. Katsas, Phys. Rev. **D88** (2013) 097501.

[10] A.V. Lipatov, M.A. Malyshev and N.P. Zotov, Phys. Lett. **B735**, 79 (2014); arXiv:1402.6481 [hep-ph].
[11] M.A. Kimber, A.D. Martin and M.G. Ryskin, Phys. Rev. **D63** (2001) 114027;
G. Watt, A.D. Martin and M.G. Ryskin, Eur. Phys. J. **C31** (2003) 73.
[12] H. Jung, G.P. Salam, Eur. Phys. J. **C19** (2001) 351;
H. Jung, arXiv:0411287 [hep-ph].
[13] ATLAS collaboration, ATLAS note, ATLAS-CONF-2013-072.
[14] K. Kutak and A.M. Stasto, Eur. Phys. J **C41** (2005) 343.
[15] K. Kutak and S. Sapeta, Phys. Rev. **D86**, 094043 (2012); arXiv:1205.5035 [hep-ph].
[16] R.K. Ellis, W.J. Stirling and B.R. Webber, "QCD and Collider Physics", Cambridge University press, Cambridge.
[17] M. Łuszczak and A. Szczurek, Eur. Phys. J. **C46** (2006) 123.
[18] F. Hautmann, Phys. Lett. B **535** (2002) 159 [hep-ph/0203140].
[19] J. Kwieciński and A. Szczurek, Nucl. Phys. **B680** (2004) 164.
[20] A.V. Lipatov and N.P. Zotov, Eur. Phys. J. **C44** (2005) 559.
[21] R.S. Pasechnik, O.V. Teryaev and A. Szczurek, Eur. Phys. J. **C47** (2006) 429.
[22] S. Marzani, R. D. Ball, V. Del Duca, S. Forte and A. Vicini, Nucl. Phys. B **800** (2008) 127 [arXiv:0801.2544 [hep-ph]].
[23] V. D. Barger and R. J. N. Phillips, Redwood City, USA: Addison-Wesley (1987) 592 P. (Frontiers in Physics, 71)
[24] J.R. Ellis, M.K. Gaillard, D.V. Nanopoulos, Nucl. Phys. B **106**, 292 (1976).
[25] A. Denner, S. Heinemeyer, I. Puljak, D. Rebuzzi and M. Spira, Eur. Phys. J. **C71**, 1753 (2011); arXiv:1107.5909 [hep-ph].
[26] A. Djouadi, J. Kalinowski and M. Spira, Comput. Phys. Commun. **108** (1998) 56.
[27] J. Beringer et al. (Particle Data Group), Phys. Rev. **D86** (2012) 010001.
[28] Y. Liao and X. Li, Phys. Lett. **B396** (1997) 225.
[29] M. Łuszczak and A. Szczurek, Phys. Rev. **D73** (2006) 054028.
[30] G.P. Lepage, J. Comput. Phys. **27**, 192 (1978).
[31] R.K. Ellis, I. Hinchliffe, M. Soldate and J.J. van der Bij, Nucl. Phys. B297 (1988) 221;
U. Baur and E.W.N. Glover, Nucl. Phys. **B339** (1990) 38.
[32] T. Figy, D. Zeppenfeld and C. Oleari, Phys. Rev. **D68** (2003) 073005.
[33] R.N. Cahn and S. Dawson, Phys. Lett. **B136** (1984) 196.
[34] M. Ciccolini, A. Denner and S. Ditmaier, Phys. Rev. **D77** (2008) 013002.
[35] P. Bolzoni, F. Maltoni, S.-O. Moch and M. Zaro, Phys. Rev. **D85** (2012) 035002.
[36] S.L. Glashow, D.V. Nanopolous and A. Yildis, Phys. Rev. **D18** (1978) 1724.
[37] V. Del Duca, W. Kilgore, C. Oleari, C. Schmidt and D. Zeppenfeld, Phys. Rev. Lett. **87** (2001) 122001; Nucl. Phys. **B616** (2001) 367.
[38] V. Del Duca, W. Kilgore, C. Oleari, C.R. Schmidt, D. Zeppenfeld, Phys. rev. **D67** (2003) 073003.
[39] V. Del Duca, G. Klämke, M.L. Mangano, M. Moretti, F. Piccinini, A.D. Polosa and D. Zeppenfeld, JHEP **0610** (2006) 016.
[40] V. Barone and E. Predazzi, "High-Energy Particle Diffraction", Springer, Berlin.
[41] G. Watt, A.D. Martin and M.G. Ryskin, Phys. Rev. **D70** (2004) 014012; erratum: ibid. **70** (2004) 079902.
[42] H. Jung and G.P. Salam, Eur. Phys. J. **C19** (2001) 351.
[43] M.A. Kimber, A.D. Martin and M.G. Ryskin, Phys. Rev. **D63** (2001) 114027.

[44] T. Pietrycki and A. Szczurek, Phys. Rev. **D75** (2007) 014023; T. Pietrycki and A. Szczurek, Phys. Rev. **D76** (2007) 034003.
[45] R. Maciuła and A. Szczurek, Phys. Rev. **D87** (2013) 094022.